Irrigation & Drainage Systems Engineering

Research Article Open Access

Hydraulics of Linear-Move Sprinkler Irrigation Systems, II: Model Development

Zerihun D[1]* and Sanchez CA[2]

[1]Maricopa Agricultural Center, University of Arizona, 37860, W. Smith-Enke Rd, Maricopa, Arizona, AZ 85138-3010, USA
[2]Department of Soil, Water, and Environmental Science and Maricopa Agricultural Center, University of Arizona, 37860 W. Smith-Enke Rd, Maricopa, Arizona, AZ 85138-3010, USA

Abstract

This manuscript presents a hydraulic simulation model for linear-move sprinkler irrigation laterals equipped with pressure reducing valves (*prvs*). The linear-move lateral considered here consists of a series of arched spans with a specified geometry and multiple outlet-ports. Lateral diameter, hydraulic resistance characteristics, field slope, spacing between outlets, and sprinkler hydraulic characteristics can be constant or variable along a lateral. Low-pressure sprinklers, or spray nozzles, coupled to pressure reducing valves are used in these laterals to achieve controlled application of irrigation water. Depending on their modes of operations, *prvs* can have a significant effect on lateral hydraulics. Thus, operating modes of *prvs* are defined and their effects on system hydraulics are described in a companion manuscript. The basic algorithms of the hydraulic computation functionality of the simulation model, presented here, are developed using techniques applicable to hydraulic manifolds. However, the algorithms developed as such are modified to account for the particular conditions that *prvs* impose on the hydraulics of a linear-move lateral. The iterative solution of the linear-move lateral hydraulic simulation problem (which typically involves multiple lateral-wide hydraulic computations) is formulated here as a one-dimensional optimization problem that seeks to minimize the error, between the computed lateral inlet head and the imposed inlet head, as a function of the distal-end nodal head. The current manuscript is part-two of a three-part article and it describes the formulation and numerical solution of the lateral hydraulic simulation problem. Part-one of the article focusses on specification of the lateral hydraulic simulation problem, statement of assumptions, and system description. Part-three presents results of model evaluation and explores potential applications of the model.

Keywords: Linear-move; Span; Manifold; *prvs; prv* operating modes; Computational modules

Notations

h_{min}: Minimum required *prv*-inlet pressure for the *prv* to function reliably in the active mode *[L]*;

h_{max}: Maximum recommended *prv*-inlet pressure for the *prv* to operate reliably in the active mode *[L]*;

h_u: *prv*-inlet (-upstream) pressure *[L]*;

prv: Pressure reducing valve *[-]*;

D: Lateral diameter *[L]*;

H: Nodal head *[L]*;

Q: Link discharge *[L^3/T]*;

Z: Nodal elevation *[L]*;

i and *j*: Link and nodal indices, respectively *[-]*;

f: Friction factor *[-]*;

p: Lateral-wide iteration index *[-]*;

ε_f and ε_r: Relative error with algebraic sign and without algebraic sign, respectively *[-]*.

Introduction

Linear-move sprinkler irrigation systems are considered among the most efficient irrigation methods [1]. They are used to irrigate a wide variety of crops, ranging from pasture to field and industrial crops, in moderately sloping fields [2]. Low-pressure sprinklers or spray nozzles coupled to pressure regulators and drop-tubes are often used in these systems to minimize energy consumption, achieve better control of water application, and reduce wind drift and spray evaporation losses. Furthermore, because of their amenability to automation linear-move systems are particularly suitable for site-specific application of water and agricultural chemicals and have minimal labor requirements. Owing to these advantages, the acreage irrigated with linear-move systems is expanding. Consequently, the development of accurate and flexible mathematical models that can be used in the hydraulic analysis, design, and management of these systems is becoming increasingly important.

Flow in irrigation laterals, including in linear-move systems, are generally considered steady. Accordingly, forms of the energy conservation and continuity equations applicable to one-dimensional steady flow in pipes can be used to describe the hydraulics of such systems [3]. Explicit analytical expressions, derived based on simplifying assumptions, were typically used to determine friction head losses and pressure distribution along solid-set and set-move sprinkler irrigation laterals [4-6]. Hydraulic modeling and design of center-pivot laterals as well relied mainly on analytical formulations or a simplified numerical approach. Kincaid and Heermann [7] presented a step-wise approach to compute pressure drop and distribution along a center-pivot lateral, assuming variable outlet discharge profile. Equations for predicting the pressure head profile of a center-pivot lateral were derived by Chu and Moe [8] considering continuous and nonuniform outflow discharge profile, constant lateral diameter, and zero slope. Scaloppi and Allen [9] extended the results of Chu and Moe by taking into account the effects of, constant slope and residual outflow discharge at the distal-

***Corresponding author:** Zerihun D, Associate Research Scientist, Maricopa Agricultural Center, University of Arizona, 37860, W. Smith-Enke Rd, Maricopa, AZ 85138-3010, USA, Tel: +15203746221, +15209828797; E-mail: dawit@ag.arizona.edu

Received May 15, 2019; **Accepted** June 10, 2019; **Published** June 17, 2019

Citation: Zerihun D, Sanchez CA (2019) Hydraulics of Linear-Move Sprinkler Irrigation Systems, II: Model Development. Irrigat Drainage Sys Eng 8: 236.

end, on lateral hydraulics. Equations for computing friction head loss in center-pivot laterals were proposed by Anwar [10], assuming constant outlet spacing and nonuniform outlet discharges as well as variable outlet spacing and constant outlet discharge. Valiantzas and Dercas [11] presented expressions for hydraulic analysis of variable diameter center-pivot laterals based on both continuous and discrete outflow assumptions. A model for design and evaluation of center-pivot systems, CPED, was presented by Heermann and Stahl [12]. Furthermore, equations for computing friction head loss in center-pivot laterals, with variable diameter, were proposed by Tabuada [13].

Published studies on hydraulic analysis of linear-move irrigation laterals are limited. A set of equations and procedure for designing linear-move irrigation systems were presented by Keller and Bleisner [5]. Fraisse et al. [14] reported the results of a simulation study on variable water application with linear-move systems. The study was conducted with a model adapted from the center-pivot evaluation and design model developed based on the earlier work of Heermann and Hein [15] and Kincaid and Heermann [7]. Existing approaches to the formulation and solution of the hydraulics of continuous-move sprinkler irrigation systems, typically, have limited flexibility in regard to their capability to accommodate variations in lateral hydraulic, geometric, and elevation profile characteristics. More importantly, most lack provisions for taking into account the effects of appurtenances such as pressure regulators, which are often used with these systems, on lateral hydraulics.

Availability of improved computational resources have allowed the development of more accurate and versatile numerical simulation models for the laterals of solid-set and set-move sprinkler irrigation systems [16-19]. These approaches can be used to develop hydraulic simulation models, of linear-move laterals, that are not limited by the constraints associated with the simplified formulations cited earlier.

The study presented here concerns the development and evaluation of a hydraulic simulation model for linear-move laterals equipped with pressure reducing valves, *prvs*. The configuration of the system, considered, and its components are described in manuscript I. Accordingly, a linear-move lateral is comprised of a concatenated series of arched spans with known geometry and multiple outlet-ports. Lateral diameter, hydraulic resistance characteristics, field slope, spacing between outlets, and sprinkler hydraulic characteristics can be constant or variable along the lateral. *prv*-sprinkler assemblies, suspended at a constant above ground clearance from the lateral outlet-ports, are used as emission devices to meter outflows at a pre-set rate along the lateral. In a well-designed and maintained system, the use of *prv*-sprinkler assemblies for precise irrigation applications should lead to a uniform and efficient application of water and agricultural chemicals along the lateral. Depending on their modes of operation, pressure reducing valves can have a significant effect on lateral hydraulics. Accordingly, the full range of the operating modes of *prvs* are defined, in the context of an irrigation lateral, and their effects on system hydraulics are described in part-one this paper.

Computational methods applicable to hydraulic manifolds are used in the development of the hydraulic computation functionality of the simulation model presented here [17]. However, the basic algorithms developed as such are modified to account for the particular conditions that *prvs* impose on the hydraulics of a linear-move lateral, as described in the companion manuscript. The solution to a lateral hydraulic simulation problem requires finding a hydraulic scenario (i.e., a combination of link discharge and nodal head vectors) with an inlet head that is sufficiently close to the imposed inlet head. Hence, it generally involves multiple iterative lateral-wide computations (sweeps), each leading to a hydraulic scenario that corresponds to a different distal-end nodal head. Thus, in order to systematize the search for the distal-end head, that corresponds to a scenario with an inlet head that is sufficiently close to the imposed head, in the model presented here the iterative solution of the linear-move lateral hydraulic simulation problem is cast as a one-dimensional optimization problem.

The current manuscript is part-two of a three-part paper and it describes the formulation and numerical solution of the hydraulic simulation problem of a linear-move lateral equipped with *prvs*. Background discussion on system configuration and components, statement of model assumptions, and specification of the lateral hydraulic simulation problem are presented in part-one of the paper. Results of model evaluation are presented and potential applications of the model are explored in the third manuscript.

System Configuration and Components, Assumptions, and Definition of the Hydraulic Simulation Problem

The specific configuration of the linear-move system, considered in the current study, and its components are described in part-one of this paper. The linear-move lateral, that is of interest here, is comprised of a series of arched spans with multiple outlet-ports placed at a constant or variable spacing. Low-pressure sprinklers, or spray nozzles, coupled to *prvs* are used to distribute irrigation water in the form of precipitation along these laterals and water is conveyed from the overhead lateral outlet-ports down to the *prv*-sprinkler assemblies through drop-tubes. Noting the significance of *prv* operating modes on lateral hydraulics, the full range of operating modes of *prvs* relevant to linear-move sprinkler irrigation laterals are defined in part-one of the current paper. Accordingly, the operating modes of *prvs* used in irrigation laterals are described as: active, passive, and fully-throttled. As will be shown shortly, the definitions of *prv* operating modes and related equations are integrated into the numerical solution presented here. Thus, for convenience, the equations that specify the operating modes of *prvs* are listed below. A *prv* is said to operate in the active mode, if

$$h_{\min} \le h_u \le h_{\max} \tag{1}$$

Where h_{min} and h_{max} are the lower and upper limits, respectively, of the recommended *prv*-inlet pressure head range for the *prv* to operate reliably in the active mode *[L]* and h_u is the upstream-end or inlet pressure of the *prv [L]*. On the other hand, a pressure reducing valve is considered to operate in the passive mode, if

$$h_u < h_{min} \tag{2}$$

and a *prv* is considered to operate in a fully-throttled mode, if

$$h_{max} < \mathrm{h_u} \tag{3}$$

Furthermore, assumptions that form the basis of the lateral hydraulic simulation model, presented here, are summarized in part-one of the current paper. Specification of the lateral hydraulic simulation problem and schematization of the linear-move lateral as a branched pipe network, consisting of links and nodes, for hydraulic analysis and simulation are also presented in the first part of this article.

Formulation and Numerical Solution of the Hydraulic Simulation Problem, Synopsis

The basic algorithms of the linear-move lateral hydraulic simulation model developed here are based on computational methods applicable to hydraulic manifolds [17]. Accordingly, the solution to the hydraulic simulation problem involves a series of iterative sweeps through each node of the lateral. Each lateral-wide hydraulic computation (iteration) begins at the distal-end junction node where an assumed initial nodal head (in the first iteration), or a revised estimate of the nodal head (in subsequent iterations), is used to compute the discharges in the attached links. Computation then proceeds upstream sequentially through each junction node, where a nodal continuity equation and link energy balance equations (forming a small nonlinear system) are solved iteratively for the nodal head and the discharges in the attached links. A lateral-wide hydraulic computation ends with the determination of the corresponding total head at the lateral inlet. At the end of each lateral-wide sweep, an error metric that measures the difference between the computed head at the lateral inlet and the actual imposed head will be compared with a preset tolerance to ascertain convergence.

If convergence is achieved, then the nodal head and link discharge vectors, $\boldsymbol{Q}$ and $\boldsymbol{H}$, computed in the current iteration will be accepted as the solution to the hydraulic simulation problem. If, on the other hand, the error in the computed lateral inlet head exceeds the tolerance, then a revised estimate of the head at the distal-end junction node is calculated and a new lateral-wide iteration is initiated. In order to systematize the search for the distal-end head that leads to a combination of $\boldsymbol{Q}$ and $\boldsymbol{H}$ vectors with an inlet-head that is sufficiently close to the imposed head, the lateral hydraulic simulation problem is cast here as a one-dimensional error minimization problem. Accordingly, in the model presented here lateral hydraulic simulations are conducted with a pair of coupled computational modules, consisting of a hydraulic module (which performs the lateral-wide iterative sweeps described above) and a one-dimensional error minimization module. In other words, the lateral hydraulic module is programmatically coupled to a one-dimensional error minimization module to form the core computational functionality of the lateral hydraulic simulation model (Figure 1). Discussion on model components and their modes of interactions will be provided shortly based on Figure 1.

Depending on the specific configuration of the linear-move system, the hydraulic module executes a lateral-wide iterative sweep following some combination of the steps outlined here:

(1) Computation of link discharges at the distal-end junction node;

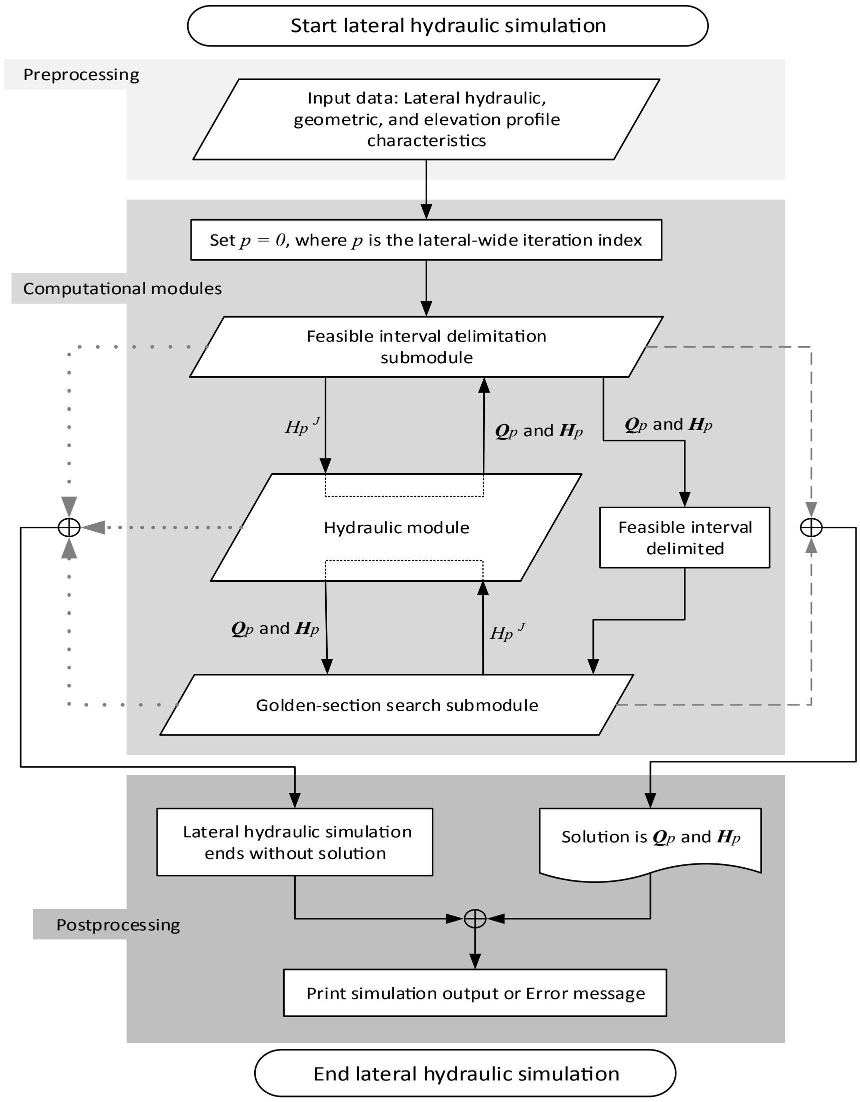

Figure 1: Flow diagram schematizing model components, modes of interactions, and directions of data flow.

(2) Iterative computation of the nodal head and link discharges at each of the offtake junction nodes upstream of the distal-end node;

(3) Computation of total head at the non-offtake junction nodes upstream of the distal-end node; and

(4) Computation of the lateral inlet head corresponding to the current lateral-wide iteration.

The one-dimensional error minimization module is comprised of two submodules:

(1) An interval bounding procedure to delimit the feasible interval of the head at the distal-end junction node and

(2) A golden-section based one-dimensional optimization (line-search) algorithm to compute the distal-end head that leads to a hydraulic scenario with an inlet head that is sufficiently close to the imposed inlet head. Note that each error minimization phase iteration involves a lateral-wide hydraulic computation. Thus, the simulation model is programmed in such way that the hydraulic computational module is embedded within the optimization algorithm.

The formulation and solution of the lateral hydraulic simulation problem as an optimization problem will now be presented in five steps. Steps 1 to 4 describe the hydraulic equations and applicable solutions in a single lateral-wide iteration. In Step 5, the lateral-wide iterative computation is cast as a one-dimensional optimization problem that seeks to minimize the error in the computed lateral inlet head.

Step 1: Equations and applicable solutions, distal-end junction node

A sketch of the distal-end and inlet-end nodes along with the intermediate junction nodes of the lateral are shown in Figure 2. Considering the distal-end junction node and the links attached to it, Figure 2a, it can be observed that the unknowns are the discharge into the node, $Q^{(I-1)}$; the distal-end drop-tube discharge, Q^{I}; and the head just upstream of the junction node, H^{J}. As noted above, in any given lateral-wide iteration an estimate of H^{J} is given, thus the unknowns are $Q^{(I-1)}$ and Q^{I}. Determination of Q^{I} and hence $Q^{(I-1)}$ needs to take into account the effects of the *prv* attached to the distal-end drop-tube.

Generally, simulation of hydraulic networks with *prvs* begins with an assumed operational mode for the *prv*s. Typically, the operating mode of *prvs* is initialized as active and then the network topology is modified in accordance with the assumption [20-22]. This would then be followed by formulation of pertinent equations and the development of applicable solution. The solution obtained as such is used either to verify or refute the assumed operational mode of the *prvs*. If the assumption is verified, then the corresponding head and discharge vector is accepted as the solution to the hydraulic simulation problem. If, on the other hand, the assumed *prv* mode of operation does not hold, then the numerical solution will point to the correct *prv* mode of operation and applicable computational alternative [20,22,23]. A similar approach will be adopted here to solve the simulation problem of irrigation laterals with *prvs*.

For irrigation laterals, the formulation and solution of the equations pertaining to an active *prv* are relatively simpler than those of a passive *prv*. Thus, starting the nodal computations with an active *prv* assumption can lead to a more efficient simulation algorithm. Accordingly, computation at the distal-end junction node will be initiated here with the presumption that the pressure reducing valve is operating in the active mode. In other words, the inlet pressure of

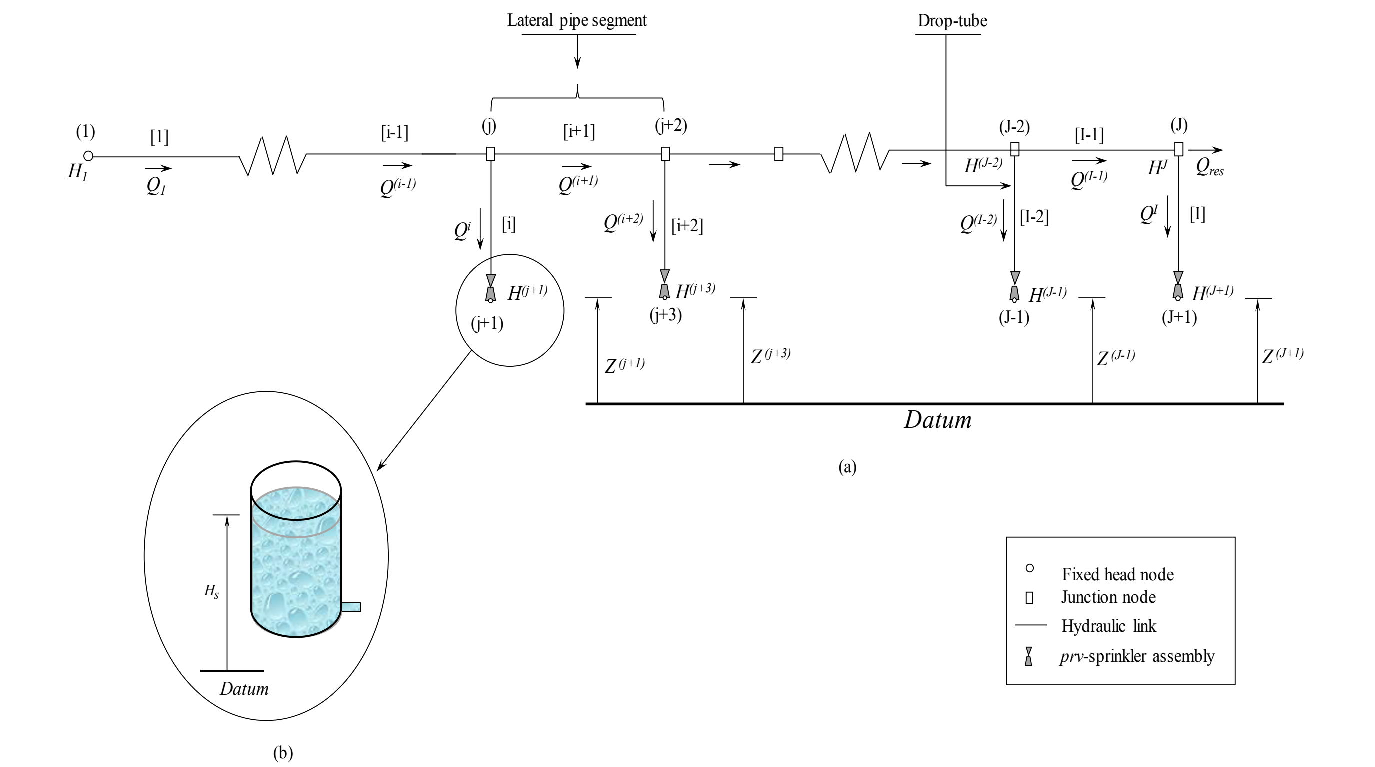

Figure 2: (a) Schematics of the inlet-end node, the distal-end junction node, and intermediate junction nodes and (b) a virtual reservoir with a constant head, H_s, equal to the sum of the *prv*-set pressure, sprinkler elevation, and velocity head at the sprinkler inlet (Note: Q^i is the *ith* link discharge; H^j and Z^j are total head and elevation, respectively, at the *jth* node; and H_s is the total head at the inlet of a sprinkler coupled with a *prv* operating in the active mode).

the distal-end *prv* is assumed to be within the range recommended for an active *prv*, eqn. (1). The implication is that the reduced pressure at the outlet of the *prv* (which is also the sprinkler inlet pressure) can be operationally considered to be the same as the *prv*-set pressure, regardless of the inlet pressure (may note discussion in Manuscript I). It can thus be readily observed that the *prv* has exactly the same effect on the sprinkler as that of a reservoir, with an equivalent constant head, installed just upstream of the sprinkler.

The preceding implies that from the perspective of computing the link discharge (i.e., the discharge through the drop-tube and *prv*-sprinkler assembly), the drop-tube has no significance and hence can be ignored. It also shows that the *prv* can be replaced by a hydraulically equivalent but conceptually more meaningful network element, specifically by a virtual-reservoir with a constant head equal to the *prv*-set pressure plus the sum of the sprinkler elevation and the velocity head at the sprinkler inlet (Figure 2b). Thus, a convenient way to look at the hydraulic condition under which a sprinkler, coupled with an active *prv*, operates is to conceptualize the sprinkler simply as a nozzle of known hydraulic characteristics plugged into the bottom of a reservoir with a fixed head. It then follows that for an active *prv*, the discharge, Q^I, of the attached sprinkler, and hence the *Ith* link, can be computed as a function of the set pressure of the *prv* independently of the system hydraulics upstream.

Once the sprinkler discharge operating under an active *prv* is computed, the active *prv* assumption can then be tested based on the computed sprinkler discharge, Q^I, and an estimate of the total head at the distal-end junction node for the current lateral-wide iteration, H^J. If the active mode assumption is verified, then the computed sprinkler discharge would be accepted and the solution proceeds to the next junction node upstream. If not, the correct operational mode of the *prv* will be determined in accordance with the criteria set earlier, eqns. (2) and (3), and an appropriate form of the flow equations will be formulated and solved.

Computation of sprinkler discharge for an active *prv* ($h_{min} \leq h_u^I \leq h_{max}$), distal-end: Based on energy balance principles, the head-discharge relationship across a sprinkler can be given as

$$H_s - Z_s = \rho Q_s^{\lambda} \tag{4}$$

where H_s is the total head at the sprinkler inlet *[L]*, Z_s is the sprinkler elevation *[L]*, Q_s is sprinkler discharge *[L³/s]*, and ρ $[T^{\lambda}L^{(1-3\lambda)}]$ and λ *[-]* are parameters of the sprinkler head-discharge function. The sprinkler parameters, ρ and λ, can be obtained based on data from sprinkler manufacturers' catalogue. Resolving the head at the sprinkler inlet, H_s, into its components (i.e., elevation, pressure, and velocity heads) and substituting the resultant expression in eqn. (4) and rearranging yields a nonlinear expression with the distal-end sprinkler, Q^I, as the unknown.

$$\rho^I \left(Q^I\right)^{\lambda^I} - \phi^I \left(Q^I\right)^2 - h_{prv} = 0 \tag{5}$$

The first term in eqn. (5) is defined in eqn. (4), the second term represents the velocity head at the sprinkler inlet, and the third term is the *prv*-set pressure. In eqn. (5), I is the link index for the distal-end drop-tube and *prv*-sprinkler assembly and ϕ^I is the coefficient of the velocity head term $[T^2/L^5]$, given as

$$\phi^I = \frac{k}{\left(D^I\right)^4} \tag{6}$$

where k is a dimensional constant whose value depends on the combination of units used $[T^2/L]$. Assuming that the diameter of the tubing between the *prv* and the sprinkler is the same as that of the attached drop-tube, D^I is set equal to the diameter of the distal-end drop-tube *[L]*.

Equation 5 can be readily solved for Q^I with a suitable iteration method. A procedure developed based on the Newton-Raphson method is used in the model presented here. The discharge of the distal-end sprinkler, Q^I, computed as such will now be used to verify the active *prv* assumption or to determine the actual mode of operation of the *prv* and decide on subsequent computational alternatives.

Verification of the active *prv* assumption, distal-end node: Verification of the active *prv* assumption is performed in two steps. First, the *prv*-inlet pressure head, that corresponds to the sprinkler discharge computed earlier based on an active *prv* assumption, is determined. The *prv*-inlet pressure is then compared with the inlet pressure range recommended for an active *prv*, eqn. (1), so as to verify or refute the assumption and decide on the computational alternatives to advance the solution further.

An expression for the inlet pressure of the *prv* attached to the distal-end drop-tube, h_u^I *[L]*, can be obtained based on the energy balance equation written over a path spanning the distal-end junction node and the inlet of the corresponding *prv*.

$$h_u^I = -\xi^I \left(Q^I\right)^2 - \phi^I \left(Q^I\right)^2 - \sum_q \pi_q^I Q^2 + H^J - Z^{(J+I)} \tag{7}$$

In eqn. (7), ξ^I is the hydraulic resistance coefficient of the friction head loss equation $[T^2/L^5]$; Q^I and ϕ^I are defined earlier in relation to eqn. (5); $\Sigma_q[.]$ is the sum of all the local head losses that occur along the distal-end drop-tube; π_q^I is the parameter of the local head loss equation for the *qth* pipe appurtenance in the *Ith* link $[T^2/L^5]$; Q is the link discharge pertinent to the *qth* local head loss component (As can be noted from eqn. (I.3) of Appendix I, depending on the source of the local head loss, Q can be the discharge upstream or downstream of an appurtenance or it can be the through-flow discharge across the appurtenance); and $Z^{(J+1)}$ is the elevation of the distal-end sprinkler (Figure 2a). Note that the elevation differential between the inlet and outlet of a *prv*-sprinkler assembly is within a few inches, thus it is considered here negligible. Accordingly, the current formulation assumes that the elevation of a sprinkler and the attached *prv* is the same.

In eqn. (7), the first term on the right hand side is the friction head loss in the distal-end drop-tube, i.e., a segment of the *Ith* link upstream of the corresponding *prv*. Noting that the Darcy-Weisbach formula is used here to calculate friction head loss in a drop-tube or a lateral pipe segment, the parameter ξ^I can be evaluated with eqn. (I.2) of Appendix I. The second term on the right-hand side of eqn. (7) is the velocity head at the *prv* inlet. The third term is the sum of the local head losses that occur within the drop-tube upstream of the *prv*, which includes local head losses due to flow division at the junction node, bending loss at the connector, and other local head loss that may occur within the drop-tube. The local head loss parameter, π_q^I, can be calculated with eqn. (I.3) of Appendix I as a function of applicable link diameter.

As noted earlier, at any given lateral-wide hydraulic computation the head just upstream of the distal-end junction node, H^J, is known. It is either an assumed initial value, in the first iteration, or a revised estimate based the results of the preceding iteration. Furthermore, the sprinkler elevation, $Z^{(J+1)}$, is specified at the input and Q^I has already been computed in the preceding step based on the assumption of an active *prv*. Depending on the pipe appurtenance considered, the link discharge, Q, in the local head loss term can be Q^I or $Q^{(I-1)}$. Thus, eqn. (7) is a function of two variables: Q^I and $Q^{(I-1)}$. However, from continuity at the distal-end junction node, it can be observed that

$$Q^{(I-1)} = Q^{I} + Q_{res} \tag{8}$$

The residual outflow at the distal-end of the lateral, Q_{res}, is considered here zero. It then follows from eqn. (8) that $Q^{(I-1)}=Q^{I}$. The implication is that eqn. (7) is a function of only Q^{I}. Considering that Q^{I} has already been computed based on the active *prv* assumption, it can be observed that the inlet pressure for the distal-end *prv*, $h_u^{\,I}$, can be calculated directly from eqn. (7). Thus, $h_u^{\,I}$ along with the recommended pressure head range for an active *prv*, defined in eqn. (1), can now be used to test the active *prv* assumption.

(1.1) Compare $h_u^{\,I}$ with h_{min}: If $h_{min} \le h_u^{\,I}$ then proceed to step 1.2. If, on the other hand, $h_u^{\,I}<h_{min}$ then proceed to 1.4.

(1.2) Compare $h_u^{\,I}$ with h_{max}: If $h_u^{\,I} \le h_{max}$ then proceed to 1.3. If, on the other hand, $h_{max}<h_u^{\,I}$ then proceed to step 1.5.

(1.3) Active mode of operation verified ($h_{min} \le h_u^{\,I} \le h_{max}$): The discharge of the distal-end sprinkler, Q^{I}, computed based on an active *prv* assumption would be accepted as the nodal solution for the current lateral-wide hydraulic computation. As noted earlier, $Q^{(I-1)}=Q^{I}$. Thus, the solution can now advance to the next junction node upstream. Considering the next node upstream, the appropriate computational procedure to execute among possible alternatives depends on the nature of the node. If the next node upstream is an offtake junction node, then the computational procedure outlined in Step 2 is applicable. On the other hand, if the node is a non-offtake node then the procedure described in Step 3 applies.

(1.4) prv is operating in the passive mode ($h_u^{\,I} < h_{min}$): As noted in the companion manuscript, a *prv* operating in a passive mode does not regulate the outlet pressure. Instead, it behaves as a fully open inline valve and its effect on the flow is limited to that of introducing some local energy loss. Under such a scenario, the attached sprinkler interacts directly with the system hydraulics upstream. Hence, for a drop-tube with a passive *prv*, the applicable form of the energy balance equation is the same as that of a drop-tube without a *prv*, except that here the local head loss that occurs across a fully open *prv* needs to be taken into account. Accordingly, the link energy balance equation written between a point just upstream of the distal-end junction node and the exit end of the distal-end sprinkler can be used to compute Q^{I}.

$$\xi^{I}\left(Q^{I}\right)^{2} + \rho^{I}\left(Q^{I}\right)^{\lambda^{I}} + \sum_{q}\pi_q^{I}Q^{2} - H^{J} + Z^{(J+1)} = 0 \tag{9}$$

Equation 9 is nonlinear in the unknown, Q^{I}, and it can be solved iteratively with a suitable procedure. An iterative algorithm based on the Newton method is implemented in the current model.

Once Q^{I} and hence $Q^{(I-1)}$ are determined, the solution advances to the junction node upstream. As noted earlier in Step 1.3, depending on the nature of the junction node upstream computation proceeds in accordance with the procedure discussed in Step 2 or 3.

(1.5) Inlet head of the prv exceeds the upper limit of the recommended range ($h_{max} < h_u^{\,I}$): When the inlet pressure of the distal-end *prv*, $h_u^{\,I}$, exceeds the recommended maximum, h_{max}, the *prv* is considered fully-throttled and hence the attached sprinkler is assumed not functional (may note discussion in manuscript I). An apparently realistic computational approach would be to set the discharge of the distal-end sprinkler to zero. However, such an approach would change the system configuration and complicates computation, especially when multiple *prvs* have inlet heads that exceed the h_{max}. Thus, the approach used here consists of one in which the effect of the *prv* is ignored and the hydraulic computation proceeds assuming a drop-tube without a *prv*. Note that under such a scenario the resultant hydraulic problem will be the same as that discussed above for a passive *prv* (Step 1.4), except that here the effect of a fully open *prv* on the flow will not be taken into account. In other words, a form of eqn. (9), that does not include the local head loss term associated with the *prv*, will be used to compute Q^{I}.

The fact that the effect of the *prv* is not taken into account may imply that computation proceeded only by ignoring a pipe appurtenance and hence the solution obtained as such cannot be considered realistic. However, it is important to note that the approach introduced here is a mere computational contrivance designed to allow the hydraulic simulation to advance forward in the current lateral-wide iteration. It is necessary, because as the lateral-wide iteration progresses it is possible that the inlet pressure of all the *prvs* in the lateral can fall below the maximum recommended pressure head for an active *prv* and hence in the eventual solution all the *prvs* could operate in the active or passive mode. Nonetheless, at the end of a hydraulic simulation, if for any one of the *prvs* in the lateral the inlet pressure, h_u, exceeds h_{max} then the solution is deemed unacceptable and a message to that effect will be printed on the screen.

Following the determination of Q^{I} and hence $Q^{(I-1)}$, computation can proceed to the junction node upstream. In accordance with the discussion in Step 1.3, the nodal head and link discharges into and from the node can be computed with the procedures described in Step 2 or 3, as the case may be.

Step 2. Equations and numerical solution, offtake junction nodes upstream of the distal-end node

The equations and computational procedure applicable to offtake junction nodes, located upstream of the distal-end node, is presented here. As noted earlier, an offtake junction node is a point along a lateral where a drop-tube (with *prv*-sprinkler assembly) is connected to an outlet port. Figure 2a depicts two consecutive offtake junction nodes upstream of the distal-end node, nodes *j* and *(j+2)*, and the link that carries discharge from node *j* to node *(j+2)*, i.e., the *(i+1)th* link. As noted earlier each lateral-wide hydraulic computation proceeds, sequentially through the junction nodes, in the upstream direction starting from the distal-end. Accordingly, the head just upstream of the *(j+2)th* node, $H^{(j+2)}$, and the discharge through the *(i+1)th* link, $Q^{(i+1)}$, would be treated here as variables whose values have been determined in the preceding computational step. The head just upstream of node *j*, H^{j}, the discharge into node *j*, $Q^{(i-1)}$, and the discharge through the drop-tube attached to node *j*, Q^{i}, would then be considered as unknowns.

The approach developed in Step 1 to take into account *prv* effects on the flow will be used here. Accordingly, first the sprinkler discharge, Q^{i}, is computed assuming an active *prv* in the *ith* link. Then $Q^{(i-1)}$ and H^{j} will be computed based on Q^{i}. Estimates of Q^{i}, $Q^{(i-1)}$, and H^{j} obtained as such are then used in the determination of the actual mode of operation of the *prv* and in the decision on how to advance the solution further.

Computation of $Q^{(i-1)}$, Q^{i}, *and* H^{j} for an active *prv* ($h_{min} \le h_u^{\,i} \le h_{max}$), offtake nodes upstream of distal-end junction node: Considering an active *prv*, the discharge of the sprinkler in the *ith* link, Q^{i}, can be calculated with a form of eqn. (5) adapted for the *ith* link. Furthermore, from continuity the discharge into node *j*, $Q^{(i-1)}$, can determined with

$$Q^{(i-1)} = Q^{i} + Q^{(i+1)} \tag{10}$$

Given $Q^{(i-1)}$, an estimate of the head just upstream of the *jth* junction node, H^{j}, can be calculated directly from an energy balance equation written over a path connecting the points just upstream of the *jth* and *(j+2)th* junction nodes.

$$H^{j} = \xi^{(i+1)}\left(Q^{(i+1)}\right)^{2} + \sum_{q}\pi_{q}^{(i+1)}Q^{2} + H^{(j+2)} \tag{11}$$

Once estimates of $Q^{(i-1)}$, Q^{i}, and H^{j} are obtained based on the active *prv* assumption, the next step is verification of the active *prv* assumption.

Verification of the active *prv* assumption, upstream of the distal-end junction node*:* For each of the offtake junction nodes upstream of the distal-end, say node *j*, the following steps are used in the verification of the active *prv* assumption or in the determination of the alternative operating modes of the *prv*.

(2.1) Compute prv inlet pressure head, $h_u^{\,i}$: The *prv*-inlet pressure in the drop-tube attached to node *j*, $h_u^{\,i}$, is calculated with a form of eqn. (7) adapted for the *ith* link. Proceed to Step 2.2.

*(2.2) Compare $h_u^{\,i}$ with h_{min}***:** If $h_{min} \le h_u^{\,i}$ then proceed to Step 2.3. If, on the other hand, $h_u^{\,i} < h_{min}$ then proceed to Step 2.5.

*(2.3) Compare $h_u^{\,i}$ with h_{max}***:** If $h_u^{\,i} \le h_{max}$ then proceed to Step 2.4. If, on the other hand, $h_{max} < h_u^{\,i}$ then proceed to Step 2.6.

(2.4) Active mode of operation verified ($h_{min} \le h_u^{\,i} \le h_{max}$): The $Q^{(i-1)}$, Q^{i}, and H^{j} computed above based on the active *prv* assumption can be accepted as the nodal solution for the current lateral-wide iteration. Computation then proceeds to the next node upstream, which would be node *j-2*. If node *j-2* is an offtake junction node, then the procedure described here, in Step 2, is applicable. If, on the other hand, node *j-2* is a non-offtake junction node, then Step 3 applies. If the computation reached the inlet-end node, then Step 4 is pertinent.

*(2.5) prv is operating in the passive mode ($h_u^{\,i} < h_{min}$)***:** As noted earlier in Step I.4, for a *prv* operating in the passive mode pertinent equations and applicable solutions have the same form as those of laterals without *prvs*. In order to solve for the unknown link discharges and nodal head (i.e., $Q^{(i-1)}$, Q^{i}, and H^{j}) a pair of link energy balance and a nodal continuity equations need to be formulated.

Accordingly, the energy balance equation between a point just upstream of the *jth* junction node and the *(j+1)th* node (which is the exit end of the corresponding sprinkler) can be obtained by adapting eqn. (9) for the *ith* link.

$$\xi^{i}\left(Q^{i}\right) \; + \rho^{i}\left(Q^{i}\right) \; + \sum \pi^{i} Q \; - H^{j} + Z^{(j \;\; 1)} = \tag{12}$$

Furthermore, the energy balance equation along the path connecting points just upstream of the *jth* and *(j+2)th* junction nodes is given in eqn. (11) and is reproduced here for convenience.

$$\sum_{q}\pi_{q}^{(i+1)}Q^{2} - H^{j} + \xi^{(i+1)}\left(Q^{(i+1)}\right)^{2} + H^{(j+2)} = 0 \tag{13}$$

and the continuity equation for the *jth* junction node is given in eqn. (10).

Some components of the local head loss terms in eqns. (12) and (13) are functions of the discharge in the *(i-1)th* link, $Q^{(i-1)}$. Now, substituting an expression for $Q^{(i-1)}$, obtained from eqn. (10), into the local head loss terms of eqns. (12) and (13) reduces the number of equations and variables each to two.

$$\xi^{i}\left(Q^{i}\right)^{2} + \rho^{i}\left(Q^{i}\right)^{\lambda^{i}} + \sum_{q}\pi_{q}^{i} f(Q^{i}) - H^{j} + Z^{(j+1)} = 0 \tag{14}$$

$$\sum_{q}\pi_{q}^{(i+1)} f(Q^{i}) - H^{j} + \xi^{(j+1)}\left(Q^{(i+1)}\right)^{2} + H^{(j+2)} = 0 \tag{15}$$

All the notations in eqns. (14) and (15), except for the expression $f(Q^{i})$ in the local head loss terms, are defined in the preceding discussions. It can be shown based on eqn. (I.3) of Appendix I and eqn. (10) that the expression $f(Q^{i})$ in eqns. (14) and (15) can have one of the following forms

$$\left.\begin{aligned} & f(Q^{i}) = \left(Q^{i}\right)^{2}, \mathit{if}\ h_{l}\ \mathit{is\ a\ function\ of}\ Q^{i}, \\ & f(Q^{i}) = \left(Q^{i}\right)^{2} + 2Q^{(i+1)}Q^{i} + \left(Q^{(i+1)}\right)^{2}, \mathit{if}\ h_{l}\ \mathit{is\ a\ function\ of}\ Q^{(i-1)} \\ & f(Q^{i}) = \left(Q^{i}\right)^{0}\left(Q^{(i+1)}\right)^{2}, \mathit{if}\ h_{l}\ \mathit{is\ a\ function\ of}\ Q^{(i+1)} \end{aligned}\right\} \tag{16}$$

where h_l refers to the local head loss component.

As can be noted from Figure 2a, eqns. (14) and (15) are the energy balance equations for the *ith* and *(i+1)th* links, respectively, expressed as functions of the total head just upstream of the *jth* junction node, H^{j}, and the discharge through the drop-tube and *prv*-sprinkler assembly attached to node *j*, Q^{i}. Equations 14 and 15 are nonlinear and hence need to be solved iteratively for H^{j} and Q^{i}. A formulation of the iterative solution of eqns. (14) and (15) is presented in Appendix II and an outline of the iterative algorithm implemented in the model is summarized in Appendix III.

Once Q^{i} and H^{j} are computed, $Q^{(i-1)}$ can be readily calculated with eqn. (10). Computation can then proceed to the next node upstream along the lateral. As stated earlier in Step 2.4, the appropriate computational alternative to execute at the next node upstream depends on the nature of the node. If the node is a junction node with a drop-tube, then the procedure described here (Step 2) is applicable. If the next node upstream is a non-offtake junction node, then Step 3 can be used to determine the nodal head. If, on the other hand, the node upstream is an inlet-end node, then Step 4 applies.

*(2.6) Inlet head of the prv exceeds the upper limit of the recommended range ($h_{max} < h_u^{\,i}$)***:** For the scenario in which the inlet pressure of the *prv* in the *ith* link, $h_u^{\,i}$, exceeds the recommended maximum, h_{max}, the *prv* is ignored and computation proceeds following the procedure outlined in Step 2.5 above for a drop-tube with a passive *prv*. However, as noted in Step 1.5, here as well the local head loss term associated with a fully open *prv* will be dropped from the energy equation. Once $Q^{(i-1)}$, Q^{i}, and H^{j} is determined, computation can then proceed to the next node upstream along the lateral. However, as described in Steps 2.4 and 2.5, above, pertinent computational procedure that needs to be executed, among possible alternatives, depends on the nature of the node upstream.

Step 3. Calculation of nodal head at a non-offtake junction node upstream of the distal-end

A non-offtake junction node is a point where two lateral pipe segments join, but it has no outlet port and hence it is not connected to a drop-tube. As described in manuscript I, if the *jth* junction node is a non-offtake node, then $Q^{i}=0$. It then follows that the discharge in the pipe segment that carries flow into the node, $Q^{(i-1)}$, is equal to the discharge in the lateral segment that carries discharge from the node, $Q^{(i+1)}$. Noting that $Q^{(i+1)}$ is known from a preceding computational step, it can then be readily observed that for a non-offtake junction node, the nodal computational problem can be reduced to one of finding the total head just upstream of the junction node, H^{j}. Accordingly, H^{j} can be determined directly from the energy balance equation for the *(i+1) th* lateral pipe segment, eqn. (11). Once H^{j} is determined computation then proceeds to the node upstream and depending on the nature of the node the procedure described here or that presented in Step 2 or

4 can be used.

Step 4. Computation of total head at the lateral inlet

At any given lateral-wide iteration, the corresponding total head at the lateral inlet can be computed with the energy balance equation written between the inlet node and the junction node immediately downstream of the lateral inlet. A form of eqn. (11) adapted for the upstream-end lateral pipe segment can be used to directly compute the head at the lateral-inlet, H^1 *[L]*, for the current lateral-wide iteration.

$$H^1 = \xi^1 \left(Q^1\right)^2 + \sum_q \pi_q^1 (Q^1)^2 + H^2 \tag{17}$$

In eqn. (17), H^2 *[L]* is the head at the junction node immediately downstream of the lateral inlet for the current lateral-wide iteration. Note that the local head loss term does not include the head loss that occurs at the lateral inlet.

Step 5. Lateral hydraulic simulation as a one-dimensional error minimization problem

Problem description: The solution to the lateral hydraulic simulation problem involves iterative computation, consisting of multiple lateral-wide sweeps, each starting at the distal-end node and ending at the inlet-end node. A lateral-wide sweep is executed using some combination of the procedures described in Steps 1 through 4 above. The goal of the iterative computation is to determine the link discharge, $\boldsymbol{Q}$, and nodal head, $\boldsymbol{H}$, vectors that lead to a lateral inlet head, H^1, that is sufficiently close to the head imposed at the lateral inlet, H_0. A computationally robust and efficient lateral-wide iterative procedure can be constructed, if the hydraulic simulation problem is cast as a one-dimensional error minimization problem. Accordingly, the hydraulic simulation problem is formulated here as an optimization problem that seeks to minimize the error in the computed inlet head as a function of the head at the distal-end junction node.

$$\boldsymbol{min}\, \varepsilon_r (H^J) = \frac{\left|H_0 - H^1(H^J)\right|}{H_0} \, subject\, to\, H^J_{min} \le H^J \le H^J_{max} \tag{18}$$

where ε_r is the normalized absolute error function of the inlet head *[-]*, and $H_{min}{}^J$ and $H_{max}{}^J$ are the lower and upper limits, respectively, of the feasible interval of H^J. Equation 18 states that the objective of optimization here is to determine the distal-end head, H^J, that minimizes the normalized absolute error function of the inlet head, ε_r *[-]*, subject to the constraint on the feasible interval of H^J.

Note that in eqn. (18) the expression $H^1(H^J)$ is a statement of the fact that for a lateral with a given hydraulic, geometric, and elevation profile characteristics, the lateral inlet head, H^1, computed in any given lateral-wide iteration is a function of the head at the distal-end node, H^J. Experience with hydraulic simulations of irrigation laterals [24] as well as intuitive reasoning suggest that H^1 is a strictly increasing function of H^J. It thus follows that the error function, ε_r, is a unimodal function of H^J. As will be shown shortly, the ε_r function and its unimodal property will be used in developing the optimization algorithm programmed into the hydraulic simulation model presented here.

The one-dimensional error minimization module: In the model presented here, a one-dimensional error minimization algorithm based on the golden-section method is used to search for the distal-end head, H^J, that leads to a hydraulic scenario with an inlet head that is sufficiently close to the imposed head. The golden-section method uses function evaluation and comparison to steadily reduce the search interval and generate a sequence of iterates, $(H_p{}^J, \varepsilon_r(H_p{}^J))$, that would eventually converge to the solution $([H^J]^*, \varepsilon_r([H^J]^*))$, where p is lateral-wide iteration index and $[H^J]^*$ is the distal-end head that minimizes the function $\varepsilon_r(H^J)$, eqn. (18). The technique is suitable for optimizing unimodal functions, which is a property of the objective function considered here. Details regarding the underlying theory, scope of application, and convergence properties of the golden-section method can be found in the optimization literature [25,26]. Thus, the discussion here will simply outline the algorithm implemented in the current model.

In order to initiate the golden-section search, first the feasible interval of H^J, $[H_{min}{}^J, H_{max}{}^J]$, needs to be defined. For a simulation problem, the potential feasible range of H^J can be defined based on hydraulic considerations. Physical requirements dictate that $H_{min}{}^J$ should exceed the elevation of the distal-end junction node of the lateral, Z^J, and $H_{max}{}^J$ should be less than the imposed inlet head, H_0. Thus, the range of variation of the head at the distal-end junction node can then be given as: $Z^J < H^J < H_0$. This observation establishes the outer limits of the interval over which H^J can vary. However, these limits are not precisely defined for the corresponding interval to be used as the feasible set over which the error function is to be minimized. Furthermore, the use of a smaller subinterval, that is a subset of the interval (Z^J, H_0), would allow a more efficient solution. Accordingly, the one-dimensional optimization (line-search) algorithm implemented in the current model is coupled with an interval delimitation subroutine designed to compute a feasible set, labeled here as *(a,d)*, which is a subset of the larger feasible interval given in eqn. (18) (Note that the notations used here to label the lower and upper limits of the feasible interval were set as such keeping in view of the properties of the golden-section search interval, which will be discussed shortly). Thus, in the current model one-dimensional error minimization computation involves two distinct phases: feasible interval delimitation and one-dimensional optimization (line-search) steps. A concise description of these phases is presented below.

I. Feasible interval delimitation phase: The goal here is to define a subset, of the larger feasible set of the error minimization problem posed in eqn. (18), that contains the solution. For convenience, the subset of the feasible set derived here will henceforth be referred to simply as the feasible set or the feasible interval. Delimitation of the feasible set is performed based on at least two lateral-wide hydraulic computations, each using a different estimate of the head at the distal-end junction node. The interval delimitation procedure starts in the first lateral-wide iteration, for which p is set to *0,* with initialization of the head at the distal-end junction node, $H_p{}^J$. The distal-end head is initialized as

$$H_p^J = z^J + \beta (H_0 - z^J)\, or\, H_p^J = z^J + \delta \tag{19}$$

whichever is larger. In eqn. (19), β *[-]* is an initial head reduction factor that vary in the range *(0,1)* and δ *[L]* is minimum required margin between Z^J and an estimate of H^J. In the model presented here, β and δ are set to 0.5 and 0.5 m, respectively. Note that the initial head needs to satisfy the constraint $Z^J < H_p{}^j < H_{max}{}^J$.

Given the initial estimate of the head at the distal-end junction node, $H_p{}^J$, the first lateral-wide iteration can now be conducted in accordance with the procedures presented earlier in Steps 1 to 4. The normalized absolute error, $\varepsilon_r([H^J])$, can then be obtained from eqn. (18) and the corresponding normalized error, $\varepsilon_f(H_p{}^J)$, can be calculated with

$$\varepsilon_f (H_p^J) = \frac{H_0 - H^1(H_p^J)}{H_0} \tag{20}$$

Note that $\varepsilon_f(H_p{}^J)$, labeled here simply as the normalized error, is the signed counterpart of the normalized absolute error function, eqn. (18). A closer look at eqn. (18) shows that the exact optimal solution, $\varepsilon_r([H^J]^*)$, is equal to 0 and it occurs when $H^1=H_0$. A feasible interval delimitation test will now be devised based on this property of the optimal solution and a comparison of the algebraic sign of the normalized error, $\varepsilon_f(H^J)$, calculated with eqn. (20) in two consecutive lateral-wide iterations. Accordingly, it will now be shown that there are two distinct sets of conditions, labeled here as *scenarios I.1* and *I.2,* under which the feasible set of the error minimization problem can be considered delimited.

Scenario I.1: This is a case in which $\varepsilon_f(H_{(p-1)}^J)>0$ and $\varepsilon_f(H_p^J)<0$. Under such a scenario, eqn. (20) shows that $H^1(H_{(p-1)}^J)<H_0$ and $H_0<H^1(H_p^J)$. An alternative, but compact restatement of these inequalities consists of

$$H_0 \in (H^1(H_{(P-1)}^J), H^1(H_p^J)) \tag{21}$$

As noted earlier the exact optimal solution, $\varepsilon_r([H^J]^*)$, is equal to 0 and it occurs when $H^1=H_0$. Thus, under *scenario I.1* the following relationship should hold

$$H^1\left(\left[H^J\right]^*\right) \in \left(H^1(H_{(p-1)}^J), H^1(H_p^J)\right) \tag{22}$$

Considering that H^1 is a strictly increasing function of H^J, it then follows that the distal-end nodal head that minimizes the normalized absolute error function, $[H^J]^*$, which is unique given the unimodal property of $\varepsilon_r(H^J)$, can be readily shown to be an element of the open set bounded by $H_{(p-1)}^J$ and H_p^J.

$$\left[H^J\right]^* \in \left(H_{(p-1)}^J, H_p^J\right) \tag{23}$$

Thus, under *scenario I.1*, the open interval $(H_{(p-1)}^J, H_p^J)$ represents the feasible set for the error minimization problem.

Scenario I.2: Consists of a case in which, $\varepsilon_f(H_{(p-1)}^J)<0$ and $\varepsilon_f(H_p^J)>0$. This scenario corresponds to $H_0<H^1(H_{(p-1)}^J)$ and $H^1(H_p^J)<H_0$, thus $H_0 \in (H^1(H_p^J),H^1(H_{(p-1)}^J))$. Following the same line of reasoning as that outlined under *scenario I.1*, above, it can be shown that under *scenario I.2* the feasible interval consists of

$$\left[H^J\right]^* \in \left(H_p^J, H_{(p-1)}^J\right) \tag{24}$$

Hence, under *scenario I.2*, the interval $(H_p^J,H_{(p-1)}^J)$ constitutes the feasible set for the error minimization problem.

Accordingly, at the end of each lateral-wide iteration, subsequent to the first, the algebraic sign of the normalized error for the current iteration, $\varepsilon_f(H_p^J)$, is compared with that of the immediately preceding iteration, $\varepsilon_f(H_{(p-1)}^J)$, to determine if the feasible interval is successfully delimited. In other words, a test is conducted to determine if the condition stated earlier in either *scenario I.1* or *I.2* (Eqns. 23 or 24) is satisfied. If the feasible interval is delimited, then the solution advances to the error minimization phase.

If, on the other hand, the algebraic sign of $\varepsilon_f(H_p^J)$ is the same as that of $\varepsilon_f(H_{(p-1)}^J)$, it then shows that depending on the relevant scenario either $[H^J]^* \notin (H_{(p-1)}^J,H_p^J)$ or $[H^J]^* \notin (H_p^J,H_{(p-1)}^J)$ and hence the solution interval is yet to be defined. In which case, a revised estimate of H^J, $H_{(p+1)}^J$, needs to be determined in order to advance the solution to the next lateral-wide iteration. A revised estimate of H^J for the next iteration is calculated with

$$H_{(p+1)}^J = H_p^J + \frac{\varepsilon_f\left(H_p^J\right)H_0}{2} \tag{25}$$

Given $H_{(p+1)}^J$ a new lateral-wide hydraulic computation is conducted and the interval delimitation test described above is executed. This process is repeated until one of the following conditions are met: *(i)* The feasible interval is delimited and hence solution can advance to the error minimization phase. Note that if *scenario I.1* holds, at the end of a successful interval delimitation phase computation, then the feasible golden-section search interval, *(a,d)*, is given as $a=H_{(p-1)}^J$ and $d=H_p^J$. If, on the other hand, *scenario I.2* holds, then $a=H_p^J$ and $d=H_{(p-1)}^J$. *(ii)* The maximum allowable number of lateral-wide iterations in the interval delimitation phase (which is equal to 30 in the current model setting) is exceeded before the feasible interval is delimited. In which case the simulation ends without a solution. or *(iii)* The lateral-wide iteration converges to the solution of the hydraulic simulation problem during the feasible interval delimitation phase. Thus, in order to account for the latter option, $\varepsilon_r(H_p^J)$ is calculated with eqn. (18) and convergence test is performed following each lateral-wide iteration. If $\varepsilon_r(H_p^J) \le \varepsilon$ (where ε is the lateral inlet head error tolerance criteria, which is set here at 0.0001), then convergence is assumed. In which case, the link discharge and nodal head vectors of the current iteration ($\boldsymbol{Q}_p$ and $\boldsymbol{H}_p$) constitute the solution.

II. One-dimensional optimization (line-search) phase

First golden-section search step: As noted in the interval bounding phase, the lower limit of the golden-section search interval, *a,* is equal to $H_{(p-1)}^J$ and the upper limit, *d,* is set to H_p^J, if *scenario I.1* of the interval delimitation phase holds. If, on the other hand, *scenario I.2* holds, then $a=H_p^J$ and $d=H_{(p-1)}^J$. Now, in order to execute a golden-section search step four points need to be defined over the feasible interval. Thus, two additional points, labeled here as *b* and *c,* need to be determined within the feasible interval, such that $a<b<c<d$. A particular property of the golden-section method is that at any given line-search step, say the *nth* search, the intermediate points are placed within the feasible interval, (a_n,d_n), such that the following ratios are satisfied

$$\alpha_1 = \frac{b_n - a_n}{d_n - a_n} = \frac{3-\sqrt{5}}{2} \approx 0.382 \quad and \quad \alpha_2 = \frac{c_n - a_n}{d_n - a_n} = \frac{\sqrt{5}-1}{2} \approx 0.618 \tag{26}$$

The theoretical basis for the definition of the constants, α_1 and α_2, per eqn. (26) can be found in the optimization literature [25,26].

It can now be shown, based on eqn. (26), that the intermediate points b_n and c_n for the first golden-section search, where *n* is set to *0*, can be calculated with

$$b_n = \alpha_1\left(d_n - a_n\right) + a_n \quad and \quad c_n = \alpha_2\left(d_n - a_n\right) + a_n \tag{27}$$

Note that the objective function values corresponding to the lower and upper limits of the search interval in the first golden-section step, (a_n,d_n), are known from the interval delimitation phase. They are given as: $\varepsilon_r(a_n)=\varepsilon_r(H_{(p-1)}^J)$ and $\varepsilon_r(d_n)=\varepsilon_r(H_p^J)$ for the case in which *scenario I.1* holds and $\varepsilon_r(a_n)=\varepsilon_r(H_p^J)$ and $\varepsilon_r(d_n)=\varepsilon_r(H_{(p-1)}^J)$, if *scenario I.2* holds. However, the objective function values of the intermediate points, $\varepsilon_r(b_n)$ and $\varepsilon_r(c_n)$, are unknowns. Thus, two consecutive lateral-wide hydraulic computations with $H_p^J=b_n$ and then $H_{(p+1)}^J=c_n$ need to be conducted to determine $H^1(b_n)$ and $H^1(c_n)$. The corresponding error function values, $\varepsilon_r(b_n)$ and $\varepsilon_r(c_n)$, can then be determined with eqn. (18).

The error function values obtained for both intermediate points, b_n and c_n, will then be tested for convergence. First the function value at b_n, $\varepsilon_r(b_n)$, is compared with the error tolerance criterion, ε, which is set to 0.0001 in the current application. Accordingly, if $\varepsilon_r(b_n) \le \varepsilon$, then convergence is assumed and the computed link discharge, $\boldsymbol{Q}_p$, and nodal head, $\boldsymbol{H}_p$, vectors corresponding to the distal-end head, b_n, will be accepted as the solution to the hydraulic simulation problem. If, on the other hand, $\varepsilon_r(b_n)>\varepsilon$, then the function value at c_n, $\varepsilon_r(c_n)$, will be tested for convergence. If $\varepsilon_r(c_n) \le \varepsilon$, then the solution to the hydraulic simulation problem is the link discharge and nodal head vectors corresponding to c_n. Conversely, if $\varepsilon_r(c_n)>\varepsilon$, then the solution advances to the next golden-section search step. Each golden-section search subsequent to the first is executed in three stages: function comparison and interval reduction, function evaluation, and convergence test. Note that subsequent discussion will be structured in accordance with this observation.

Function comparison and feasible interval reduction: Any given golden-section search (say the *(n+1)th* step) begins with a comparison of the normalized absolute errors, at the intermediate points, of the preceding (i.e., the *nth*) golden-section search step. In other words, the *(n+1)th* step begins by comparing $\varepsilon_r(b_n)$ with $\varepsilon_r(c_n)$. Function comparison can lead to one of the following two distinct outcomes: a scenario where $\varepsilon_r(b_n) \le \varepsilon_r(c_n)$, labeled here as *scenario II.1*, or one in which $\varepsilon_r(c_n)<\varepsilon_r(b_n)$, defined here as *scenario II.2*.

First consider a case in which *scenario II.1* [i.e., $\varepsilon_r(b_n) \le \varepsilon_r(c_n)$] holds. Noting that ε_r is a unimodal function of H^J, it can then be readily reasoned that the subinterval $[c_n,d_n)$ does not contain the minimum point of the function, i.e., $[H^J]^* \notin [c_n,d_n)$. Thus, the search interval for the next golden-section step can be reduced to (a_n,c_n). Accordingly, the interval for the *(n+1)th* iteration can be given as:

$$a_{(n+1)} = a_n \quad and \quad d_{(n+1)} = c_n \tag{28}$$

Furthermore, if $c_{(n+1)}$ is set equal to b_n and $b_{(n+1)}$ is defined as

$$b_{(n+1)} = \alpha_1 \left(d_{(n+1)} - a_{(n+1)} \right) + a_{(n+1)} \tag{29}$$

it can then be shown that the placement of the intermediate points, $b_{(n+1)}$ and $c_{(n+1)}$, within the reduced interval $(a_{(n+1)},d_{(n+1)})$ conforms to the requirements stated in eqn. (26).

Alternatively, if $\varepsilon_r(c_n)<\varepsilon_r(b_n)$ (i.e., if *scenario II.2* holds), then the search interval for the next golden-section step can be reduced to (b_n,d_n). Accordingly, the interval for the *(n+1)th* step becomes

$$a_{(n+1)} = b_n \quad and \quad d_{(n+1)} = d_n \tag{30}$$

In addition, if $b_{(n+1)}$ is set equal to c_n and $c_{(n+1)}$ is defined as

$$c_{(n+1)} = \alpha_2 \left(d_{(n+1)} - a_{(n+1)} \right) + a_{(n+1)} \tag{31}$$

then the placement of points, $b_{(n+1)}$ and $c_{(n+1)}$, within the reduced interval $(a_{(n+1)},d_{(n+1)})$ will satisfy the requirements stated in eqn. (26). Once the feasible interval and the intermediate points for the current golden-section search are determined computation then proceeds to the next stage, which involves evaluation of the normalized absolute error function at each of these points.

Function evaluation: Considering the case in which function comparison shows that $\varepsilon_r(b_n) \le \varepsilon_r(c_n)$ (i.e., if *scenario II.1* holds), then from eqns. (28) and (29) it can be readily inferred that

$$\varepsilon_r(a_{(n+1)}) = \varepsilon_r(a_n),\ \ \varepsilon_r(c_{(n+1)}) = \varepsilon_r(b_n),\ \ and\ \ \varepsilon_r(d_{(n+1)}) = \varepsilon_r(c_n) \tag{32}$$

However, the function value at the intermediate point $b_{(n+1)}$, which is a point generated in the current iteration, is unknown. Thus, a lateral-wide hydraulic computation needs to be conducted with $H_p^J=b_{(n+1)}$ to determine $H^1(b_{(n+1)})$. The corresponding normalized absolute error, $\varepsilon_r(b_{(n+1)})$, will then be calculated with eqn. (18).

Alternatively, if function comparison showed that $\varepsilon_r(c_n)<\varepsilon_r(b_n)$ (i.e., if *scenario II.2* holds), then it follows from eqns. (30) and (31) that

$$\varepsilon_r(a_{(n+1)}) = \varepsilon_r(b_n),\ \ \varepsilon_r(b_{(n+1)}) = \varepsilon_r(c_n),\ \ and\ \ \varepsilon_r(d_{(n+1)}) = \varepsilon_r(d_n) \tag{33}$$

The function value at the intermediate point $c_{(n+1)}$ is unknown. Thus, a lateral-wide hydraulic computation will be conducted with $H_p^J=c_{(n+1)}$ to determine $H^1(c_{(n+1)})$. The corresponding normalized absolute error, $\varepsilon_r(c_{(n+1)})$, will then be calculated with eqn. (18).

Once the error function is evaluated at the newly generated intermediate point (which could be either $b_{(n+1)}$ or $c_{(n+1)}$, depending on the relevant scenario), computation can then proceed to the next stage.

Convergence test: At the end of a golden-section search step a convergence test is conducted. Convergence is assumed, if $\varepsilon_r(b_{(n+1)}) \le \varepsilon$ for the case in which *scenario II.1* holds or if $\varepsilon_r(c_{(n+1)}) \le \varepsilon$ for the case in which *scenario II.2* holds. Either way, the link discharge and nodal head vectors, $\boldsymbol{Q}_p$ and $\boldsymbol{H}_p$, obtained in the current lateral-wide hydraulic computation would constitute the solution to the simulation problem. Conversely, if the computed normalized absolute error is greater than the preset tolerance (i.e., if $\varepsilon_r(b_{(n+1)})>\varepsilon$ for *scenario II.1* or $\varepsilon_r(c_{(n+1)})>\varepsilon$ for *scenario II.2*), then computation proceeds to the next golden-section search step and the procedure outlined above (consisting of function comparison and interval reduction, function evaluation, and convergence test phases) will be repeated. Minimization of the error function, eqn. (18), continues until either convergence is achieved or a specified maximum number of searches (which is set to 50 in the current model) is exceeded, in which case the computation ends without a solution.

It can be readily shown, based on eqns. (28)-(31), that if the placement of the intermediate points within the first search interval satisfy the requirements specified in eqn. (26), then the placement of the intermediate points for all subsequent iterations will automatically satisfy these requirements. Although four points are needed to execute a golden-section search step, it needs to be noted that only one new function evaluation is required in all but the first iteration. In theory, the golden-section method has a lower rate of convergence than other more widely used methods, such as the Newton method [25,26]. However, the fact that the golden-section method does not require evaluation of derivatives makes it suitable for optimizing problems in which the objective function and the decision variable cannot be related in terms of a simple functional expression.

Highlight of Model Inputs and Outputs, Model Components, and Their Modes of Interactions

Highlight of model inputs and outputs

The linear-move lateral hydraulic simulation model presented here is implemented in a C++ program developed based on the object oriented approach. The model produces a range of outputs given the hydraulic, geometric, and elevation data of a linear-move sprinkler irrigation system as input. The specific input data items include lateral pipe segment lengths and lateral elevation profiles (both defined along the centerline of a lateral), lateral diameter, pipe relative roughness, drop-tube lengths and diameters, *prv* parameters, outlet spacing, sprinkler parameters, local head loss coefficients, and total head at the lateral inlet. The main outputs of the numerical model are the link discharge vector (lateral pipe segment and sprinkler discharges), $\boldsymbol{Q}$, and total heads just upstream of each junction node, $\boldsymbol{H}$. Additional model outputs include velocity heads and friction head losses in each of the lateral pipe segments, local head losses, piezometric head profile along the lateral, lateral pressure head profile, inlet and outlet pressures of each *prv*, *prv* operating modes (active and/or passive), and head differential across each sprinkler.

Components of the lateral hydraulic simulation model and their modes of interaction

The main elements of the hydraulic simulation model, their modes of interaction, and the directions of data flow are depicted in a simplified flow diagram schematized in Figure 1. Based on a theme of model functionality, model components are categorized here into three elements: pre-processing, computation, and post-processing (Figure 1). Note that varied background shedding is used in Figure 1 to differentiate between the program components.

Pre-processing and post-processing: The pre-processing and post-processing model components are shown in the top and bottom boxes of Figure 1 and they represent model functionalities that relate to the processing of input and output data, respectively.

Computation: As noted earlier, the lateral hydraulic simulation problem is cast here as a one-dimensional error minimization (optimization) problem. Given a lateral parameter set, the objective of the optimization problem is one of finding the distal-end nodal head, H^J, that leads to a combination of link discharge and nodal head vectors, $\boldsymbol{Q}$ and $\boldsymbol{H}$, with an inlet head that is sufficiently close to the imposed head (i.e., the lateral inlet head specified at the input). Accordingly, in the model presented here hydraulic simulation computations are conducted using a pair of coupled modules, consisting of a hydraulic module (which performs a lateral-wide iterative sweep through each node of the lateral) and a one-dimensional error minimization module. As will be shown shortly, each one-dimensional error minimization computational step (iteration) involves at least one function call to the hydraulic module. Thus, programmatically speaking, the hydraulic module is embedded within the error minimization module. The error minimization module itself is comprised of two submodules: a feasible interval delimitation submodule and a one-dimensional optimization (line-search) algorithm developed based on the golden-section method, which is simply termed in Figure 1 as a golden-section search submodule.

As can be noted from Figure 1, hydraulic simulation computations start in the feasible interval delimitation submodule. The interval delimitation submodule determines the feasible set of the independent variable, H^J, of the error minimization problem. In order to successfully delimit the feasible interval of the distal-end nodal head, the interval delimitation submodule invokes the hydraulic module at least twice, typically multiple times. In each function call, the interval delimitation submodule passes the value of the distal-end nodal head for the current iteration (H_p^J), which is an assumed initial value determined in accordance with eqn. (19) (in the first iteration) or a revised estimate of the nodal head (in subsequent iterations), to the hydraulic module (Figure 1). The hydraulic module then performs a lateral-wide sweep that starts at the distal-end node and ends at the inlet-end node of the lateral. In a lateral-wide sweep, if any of the nodal iterative computations fail to converge, then the hydraulic simulation will end without a solution, as shown in Figure 1 with a dotted-line. A successful lateral-wide hydraulic computation, on the other hand, ends with the determination of the link discharge and nodal head arrays corresponding to H_p^J. The hydraulic module then returns the link discharge and nodal head arrays computed in the current iteration, $\boldsymbol{Q}_p$ and $\boldsymbol{H}_p$, to the interval delimitation submodule.

The feasible interval delimitation submodule then performs convergence test (in accordance with the criterion describe earlier) to determine if the inlet head computed in the current iteration is sufficiently close to the imposed head. If convergence is achieved, then the link discharge and nodal head arrays computed in the current iteration, $\boldsymbol{Q}_p$ and $\boldsymbol{H}_p$, will be accepted as the solution to the hydraulic simulation problem. The $\boldsymbol{Q}_p$ and $\boldsymbol{H}_p$ arrays will be passed, as shown in Figure 1 with a dashed-line, to the post-processing model functionality where output data will be saved in output data files. Note that the interval delimitation submodule is not specifically designed to determine the solution to a hydraulic simulation problem, thus to the extent that convergence occurs within the interval delimitation phase it is only incidental and hence it is not a typical computational outcome.

If, on the other hand, convergence test returns false, then the interval delimitation submodule calculates a revised estimate of the distal-end nodal head in accordance with eqn. (25). The hydraulic module is then invoked and a new lateral-wide computation based on the revised estimate of the head at the distal-end node, H_p^J, will be executed. These steps are repeated until either the maximum allowable number of interval delimitation iterations are exceeded, in which case simulation ends without a solution (Figure 1), or the feasible interval of H^J is delimited. Once the feasible interval is bounded, then discharge and nodal head arrays computed in the current iteration, $\boldsymbol{Q}_p$ and $\boldsymbol{H}_p$, will be passed to the golden-section search submodule.

A line-search algorithm developed based on the golden-section method is used here to systematically search, within the feasible interval, for the distal-end nodal head that minimizes the normalized absolute error between the computed and the imposed inlet heads, eqn. (18). In a golden-section search step, the golden-section submodule invokes the hydraulic module, at least once, and passes the value of the distal-end nodal head for the current iteration, H_p^J. The hydraulic module then performs a lateral-wide sweep to determine the nodal head and discharge arrays corresponding to the current distal-end nodal head. Following a successful lateral–wide hydraulic computation, the lateral hydraulic module returns the computed discharge and head vectors, $\boldsymbol{Q}_p$ and $\boldsymbol{H}_p$, to the golden-section search submodule (Figure 1).

The golden-section search submodule will then perform convergence test using the criterion described earlier. If convergence test returns true, then the link discharge and nodal head vectors computed in the current golden-section search step will be accepted as the solution to the hydraulic simulation problem. The $\boldsymbol{Q}_p$ and $\boldsymbol{H}_p$ vectors will then be passed, as shown in Figure 1 with a dashed-line, to the post-processing model functionality where model outputs are processed. If, on the other hand, the golden-section search step did not converge, then a revised estimate H^J will be determined in accordance with the golden-section procedure and a new lateral-wide iteration is initiated. This process is repeated until either a specified number of maximum allowable iterations are exceeded, in which case program ends without a solution, or a solution is obtained.

Discussion and Conclusions

A hydraulic simulation model is developed for linear-move sprinkler irrigation laterals equipped with pressure reducing valves, *prvs*. The linear-move lateral considered here consist of a series of arched spans with a specified geometry and multiple outlet-ports. The lateral hydraulic and geometric characteristics can be constant or variable along the lateral. In order to maintain a pressure sufficiently close to a suitably selected set pressure upstream of the sprinklers, each sprinkler is coupled to a *prv* at its inlet-end. Operating modes of *prvs* determine *prv*-effects on lateral hydraulics. Accordingly, the full range of *prv* operational modes are defined, in the context an irrigation lateral, and their effects on lateral hydraulics is described in a companion manuscript. The definition of the operating modes of *prvs* and pertinent equations are then integrated into the formulation and numerical solution of the hydraulic simulation model presented here.

Computational methods applicable to hydraulic manifolds form the basis of the numerical algorithms of the hydraulic computation functionality of the simulation model. However, the basic algorithms developed as such are modified to account for the effects of *prvs* on the hydraulics of a linear-move lateral. The solution to a hydraulic simulation problem requires the determination of a hydraulic scenario (i.e., a combination of link discharge and nodal head arrays) with an inlet head that is sufficiently close to the imposed head. Hence, it generally involves multiple lateral-wide iterative sweeps, each leading to a hydraulic scenario that corresponds to a different distal-end nodal head. Thus, in order to systematize the search for the distal-end head, that corresponds to a hydraulic scenario with an inlet head that is sufficiently close to the imposed head, the linear-move lateral hydraulic simulation problem is formulated here as a one-dimensional optimization problem. Accordingly, a line-search algorithm, developed based on the golden-section method, is used in the model presented here to minimize the normalized absolute error, between the computed lateral inlet-head and the imposed head, as a function of the distal-end nodal head of the lateral.

This manuscript presents the formulation and numerical solution of the hydraulic simulation problem of a linear-move lateral equipped with *prvs*. The companion manuscripts present system description, model assumptions, specification of the hydraulic simulation problem, and model evaluation.

References

1. Keller J, Corey F, Walker WR, Vavra ME (1980) Evaluation of Irrigation Systems. In Irrigation: Challenges of the 80's. Proceedings of the Second National Irrigation Symposium, 95-105, St. Joseph, MI, ASAE.
2. Gregg T (2004) Water Conservation Best Management Practice Guide, Report 362, Texas Water Development Board, Austin, Texas.
3. Granger RA (1995) Fluid Mechanics. Dover Publications Inc., New York, NY.
4. Christiansen JE (1942) Irrigation by Sprinkling. California Agricultural Experiment Station Bulletin, 670, University of California, Davis, CA.
5. Keller J, Bliesner R (1990) Sprinkle and trickle irrigation. Van Nostrand Reinhold, New York, NY.
6. Martin DL, Heermann DF, Madison M (2007) Design and Operation of Farm Irrigation Systems. In: Hoffmans GJ, Evans RG, Jensen ME, Martin DL, Elliott RL, (2nd eds.) Hydraulics of Sprinkler and Micro-Irrigation Systems American Society of Agricultural and Biological Engineers Chapter 15, pp. 532-556.
7. Kincaid DC, Heermann DF (1970) Pressure Distribution on a Center-Pivot Sprinkler Irrigation System. Trans ASAE, 13(5):556-558.
8. Chu ST, Moe DL (1972) Hydraulics of a Center Pivot System. Amer Soc Agr Eng Trans ASAE, 15(5):894-896.
9. Scaloppi EJ, Allen RG (1993) Hydraulics of Center-Pivot Laterals. J Irrig Drain Eng ASCE, 119(3): 554-567.
10. Anwar AA (1999) Friction Correction Factors for Center-Pivots. J Irrig Drain Eng ASCE, 125(5): 280-286.
11. Valiantzas JD, Dercas N (2005) Hydraulic Analysis of Multidiameter Center-Pivot Sprinkler Laterals. J Irrig Drain Eng ASCE, 131(2): 137-142.
12. Heermann DF, Stahl KM (2006) CPED: Center Pivot Evaluation and Design Center for Agricultural Resources Research, Water Management and Systems Research, USDA.
13. Tabuada MA (2014) Friction Head Loss in Center-Pivot Laterals with Single Diameter and Multidiameter. J Irrig Drain Eng ASCE 140(10): 04014033.
14. Fraisse CW, Heermann DF, Duke HR (1995) Simulation of Variable Water Application with Linear-Move Irrigation System. Transactions of the ASAE, 38(5):1371-1376.
15. Heermann DF, Hein PR (1968) Performance Characteristics of Self-Propelled Center- Pivot Sprinkler Irrigation System. Trans ASAE, 11(1):11-15.
16. Hathoot HM, Abo-Ghobar HM, Al-Amud AI, Mohammad FS (1994) Analysis and Design of Sprinkler Irrigation Laterals. J Irrig Drain Eng ASCE, 120(3):534-549.
17. Zerihun D, Sanchez CA, Nolte K (2014) Field-scale Sprinkler Irrigation Hydraulic Model. I. Hydraulic Characterization. J Irrig Drain Eng 140(7): 04014019.
18. Zerihun D, Sanchez CA (2014) Field-Scale Sprinkler Irrigation Hydraulic Model. 1100 II: Hydraulic Simulation. J Irrig Drain Eng 140(7): 04014020.
19. Zerihun D, Sanchez CA (2017) Irrigation Lateral Hydraulics with the Gradient Method. J Irrig Drain Eng ASCE 143(8): 04017023.
20. Jeppson RW (1976) Analysis of flow in pipe networks. Butterworth Publishers, Boston, MA.
21. Jeppson RW, Davis AL (1976) Pressure Reducing Valves in Pipe Network Analyses. J Hydraul Div ASCE, 102(7): 987-1001.
22. Larock BE, Jeppson RW, Watters GZ (1999) Hydraulics of Pipeline Systems. CRC Press, Washington, DC.
23. Behave PR, Gupta R (2006) Analysis of Water Distribution Networks. Alpha Science International Ltd., Oxford, UK.
24. Zerihun D, Sanchez CA (2012) Sprinkler model: A field-scale solid set sprinkler irrigation hydraulic model, Program documentation.
25. Avriel M (1976) Nonlinear Programming: Analysis and Methods. Prentice Hall Inc., Englewood cliffs, NJ.
26. Beightler CS, Phillips DT, Wilde DJ (1979) Foundations of Optimization. Prentice-Hall, Inc., Englewood Cliffs, NJ.
27. Lipschutz S (1991) Theory and problems of linear algebra. Schaum's Outline Series, 2nd edition, McGraw-Hill, Inc., New York, NY.Y.

Appendix I. Equations for friction and local head loss terms

Friction head loss, h_f *[L]*, in a hydraulic link (i.e., a lateral pipe segment or a drop-tube) can be expressed as

$$h_f = \xi Q^2 \qquad (I.1)$$

In Eq. I.1, ξ is the hydraulic resistance coefficient of the friction head loss equation $[T^2/L^5]$ and Q is link discharge $[L^3/T]$. Note that for convenience, in Eq. I.1 the hydraulic resistance coefficient, ξ, and the link discharge, Q, are written without the link index.

Noting that the Darcy-Weisbach formula is used to calculate friction head loss in the current model, ξ can be given as

$$\xi = k_f \frac{f}{D^5} l \qquad (I.2)$$

where k_f is a dimensional constant in the friction head loss equation $[T^2/L]$; f is the friction factor for a hydraulic link *[-]*; l is the link length *[L]*; and D is the link diameter *[L]*.

In the model presented here, for $R \le 4000$, where R is the Reynolds number, the link friction factor, f, is calculated with the friction factor formula applicable to laminar flow in pipes. For turbulent flow ($4000 < R$), f is computed through iterative solution of the Colebrook-White equation. The exact form of the Colebrook-White equation used in the model presented here is given by Zerihun and Sanchez (2017).

Furthermore, the local head losses, h_l *[L]*, across pipe transitions (such as pipe size changes, fittings, tees, elbows, valves) where the flow is constrained, changes direction, or changes velocity are calculated with

$$h_l = \pi Q^2, \quad where \quad \pi = k_l \frac{k_L}{D^4} \qquad (I.3)$$

In Eq. I.3, π is local head loss parameter $[T^2/L^5]$, k_l is a dimensional constant $[T^2/L]$, and k_L is the local head loss coefficient of an appurtenance *[-]*. Note that depending on the source of the local head loss, the link discharge, Q, and diameter, D, applicable to Eq. I.3 could be those corresponding to the link carrying discharge into the pipe appurtenance that caused the head loss or the link that carries discharge from it. Alternatively, for appurtenances across which link discharges and diameters are the same, the through-flow discharge and the local link diameter is used in these equations.

Appendix II. Formulation of the iterative solution of Eqs. 14 and 15

Equations 14 and 15 are nonlinear in the unknowns, Q^i and H^j, and need to be solved iteratively. In order to formulate the iterative solution, Eqs. 14 and 15 will now be expressed as

$$F_1(Q^i, H^j) = \xi^i \left(Q^i\right)^2 + \rho^i \left(Q^i\right)^{\lambda^i} + \sum_q \pi_q^i f(Q^i) - H^j + Z^{(j+1)} \qquad (II.1)$$

$$F_2(Q^i, H^j) = \sum_q \pi_q^{(i+1)} f(Q^i) - H^j + \xi^{(i+1)} \left(Q^{(i+1)}\right)^2 + H^{(j+2)} \qquad (II.2)$$

where functions $F_1(Q^i, H^j)$ and $F_2(Q^i, H^j)$ represent, respectively, the residuals of energy balance over the *ith* and *(i+1)th* links in an iteration. An iterative algorithm developed based on the Newton method is used here to solve Eqs. II.1 and II.2 for Q^i and H^j. Accordingly, at any given iteration, say at the *(m+1)th* iteration (where *m* is the iteration index), the incremental changes in Q^i and H^j is computed through the simultaneous solution of a pair of linear equations, which can be expressed in vector form as

$$\zeta_m \delta x_{(m+1)} = -F_m \qquad (II.3)$$

For convenience, in subsequent development the variables in Eqs. II.1 and II.2 (i.e., Q^i and H^j) will be written without the link and nodal indices. Accordingly, the notations $\boldsymbol{\zeta}_m$, $\delta\mathbf{x}_m$, and $\mathbf{F}_m$, in Eq. II.3, can be expressed as

$$\boldsymbol{\zeta}_k = \begin{pmatrix} \left.\dfrac{\partial F_1}{\partial Q}\right|_{Q_m} & \left.\dfrac{\partial F_1}{\partial H}\right|_{H_m} \\ \left.\dfrac{\partial F_2}{\partial Q}\right|_{Q_m} & \left.\dfrac{\partial F_2}{\partial H}\right|_{H_m} \end{pmatrix}, \quad \delta\mathbf{x}_{m+1} = \begin{pmatrix} \delta Q_{(m+1)} \\ \delta H_{(m+1)} \end{pmatrix}, \; and \;\; \mathbf{F}_m = \begin{pmatrix} F_1(Q_m, H_m) \\ F_2(Q_m, H_m) \end{pmatrix} \qquad (II.4)$$

In Eq. II. 4, $\boldsymbol{\zeta}_m$ is a coefficient matrix evaluated based on Q_m and H_m (Note that the first and second rows of $\boldsymbol{\zeta}_m$ represent the transpose of the gradient vectors of F_1 and F_2, respectively, at the *mth* iteration); Q_m and H_m are estimates of the *ith* link discharge and the head just upstream of the *jth* junction node at the *mth* iteration, respectively; $\delta\mathbf{x}_{(m+1)}$ is vector of the incremental changes in the unknowns in the *(m+1)th* iteration; and $\mathbf{F}_m$ is the residual vector evaluated based Q_m and H_m. Note that details regarding the evaluation of the derivatives of the functions F_1 and F_2 with respect to Q and H, Eq. II.4, are presented by Zerihun and Sanchez (2017).

Appendix III. Iterative algorithm for the solution of Eqs. 14 and 15

Iterative solution of Eqs. 14 and 15 for the *ith* link discharge, Q^i, and the *jth* junction node, H^j, is outlined here. For simplicity, in subsequent discussion the *ith* link discharge at the *mth* iteration, Q_m^i, and the *jth* nodal head at the *mth* iteration, H_m^j, will be written without the link and nodal indices simply as Q_m and H_m, respectively.

1. Set $m = 0$ and initialize Q_m and H_m. A good initial approximation consists of setting Q_m equal to the discharge of the nearest sprinkler downstream of the current sprinkler and H_m equal to the head at the nearest junction node, with an outlet port, downstream of the current node. Proceed to step 2.
2. Compute elements of the residual vector, $\mathbf{F}_m$, as a function of Q_m and H_m (Eqs. II.1 and II.2). Proceed to step 3.
3. Compute elements of the coefficient matrix, $\boldsymbol{\zeta}_m$, (Eq. II.4) based on Q_m and H_m. Proceed to step 4.
4. Compute the incremental change in the variable vector in the current iteration, $\delta\mathbf{x}_{(m+1)}$, Eq. II.3. Proceed to step 5. [Note that in the current model, Eq. II.3 is solved for $\delta\mathbf{x}_{(m+1)}$ with Cramer's rule (e.g., Lipschutz, 1991)].
5. Update variables: set $Q_{(m+1)} = Q_m + \delta Q_{(m+1)}$ and $H_{(m+1)} = H_m + \delta H_{(m+1)}$. Proceed to step 6.
6. Convergence test:

   6a. If $|\delta Q_{(m+1)}|/Q_{(m+1)} \leq 10^{-7}$, then proceed to step 6b. If not proceed to step 7.

   6b. If $|\delta H_{(m+1)}|/H_{(m+1)} \leq 10^{-7}$, then proceed to step 10. If not, proceed to step 7.
7. Set $m = m+1$, proceed to step 8.

8. If $m \leq$ *MaximumNodalIteration*, then proceed to step 2. If, on the other hand, *MaximumNodalIteration* $< m$, then proceed to step 9. (Note: *MaximumNodalIteration* is the maximum allowed number of nodal iterations, which is set to 30 in the current model)

9. Iterative computation of the total head just upstream of the *jth* junction node, H^{j}, and the discharge in the attached drop-tube and *prv*-sprinkler assembly (i.e., the *ith* link), Q^{i}, failed to converge. End computation.

10. The total head just upstream of the *jth* junction node and the discharge in the attached drop-tube and *prv*-sprinkler assembly (i.e., the *ith* link) for the current lateral-wide iteration has been computed and it can be given as: $Q^{i} = Q_{(m+1)}$ and $H^{j} = H_{(m+1)}$. End nodal computation.